Journal of New Materials for Electrochemical Systems 15, 215-223 (2012)
© J. New Mat. Electrochem. Systems

Production of Hydrogen from Ethanol Using Pt/Hydrotalcite Catalysts Stabilized with Tungsten Oxides

J.L. Contreras[*,1], M.A. Ortiz[1], R. Luna[1], G.A. Fuentes[2], M. Autié[3], J. Salmones[4], B. Zeifert[4], M. Gordon[1] and T. Vázquez[5]

[1]Universidad Autónoma Metropolitana-Azcapozalco CBI, Energía, Av. Sn.Pablo 180 Col.Reynosa C.P.02200 México D.F., México.
[2] Universidad Autónoma Metropolitana-Iztapalapa CBI, IPH, México, D.F., México
[3]Instituto de Ciencia y Tecnología de Materiales, Universidad de la Habana, La Habana, Cuba and
Facultad de Ingeniería Química.Instituto Superior Politécnico José Antonio Echeverria, FQB-MES.La Habana Cuba
[4] Instituto Politécnico Nacional, ESIQIE,Unidad Prof. ALM, México, D. F., 07738, México
[5]Instituto Mexicano del Petróleo, Eje Central Lázaro Cárdenas 152, México, D.F., México

Received: November 25, 2011, Accepted: February 10, 2012, Available online: April 16, 2012

Abstract: *An stabilization effect of WOx over the Pt/hydrotalcite catalysts to produce H_2 by ethanol steam reforming at low concentration was studied. The catalysts were characterized by N_2 physisorption, X-ray diffraction, Infrared (IR), and UV-vis spectroscopy. The catalytic tests were made in a fixed bed reactor. The catalysts showed porous with the shape of parallel layers with a monomodal mesoporous distribution. By IR spectroscopy it was found superficial chemical such as: -OH, H_2O, Al-OH, Mg-OH, and CO_3^{2-}. The reaction products were; H_2, CO_2, CH_3CHO, CH_4 and C_2H_4. These catalysts did not produce CO and showed low selectivity to C_2H_4. By XRD we found that catalysts having Pt and the lowest W concentration showed the highest crystallinity and the highest stability during the reaction of ethanol steam reforming. A possible thermal stabilization effect of W in the hydrotalcite crystal structure leading to prevent the Pt sintering is proposed. By IR the hydrotalcite hydroxil groups coordinated with Mg and Al decreased by the presence of WOx. We found that catalysts with low W concentration and Pt having high crystallinity showed the highest stability after ethanol steam reforming. It could be a possible thermal stabilization effect of W in the hydrotalcite crystal structure leading to prevent the Pt sintering.*

Keywords: Hydrogen, WOx, Hydrotalcite, catalysts, Platinum, ethanol

1. INTRODUCTION

In order to produce hydrogen and its potential use in fuel cells, it has been proposed bioethanol as a source using the catalytic steam reforming. Bioethanol possesses diverse advantages over the derived hydrocarbons of fossil sources, it comes from renewable sources and it is neutral with respect to emissions of CO_2, less toxic and it can be stored without handling risk. It can be obtained in large quantities from biomass in comparison with methanol and gasoline.

The reaction of ethanol with steam is strongly endothermic and it only produces H_2 and CO_2 if the ethanol reacts in the most desirable way. However, other undesirable products such as CO and CH_4 are also in general formed during the reaction [1]. Other reactions occur such as ethanol dehydrogenation to CH_3CHO, dehydration to $CH_2{=}CH_2$, decomposition to CO and CH_4 or CO_2, CH_4 and H_2. The CH_3CHO and the $CH_2{=}CH_2$ are intermediary products that could be formed during the reaction at relatively low temperatures before the formation of H_2 and CO_2 and finally the formation of coke over the surface of the catalyst.

For this reaction, some authors [2-3] have demonstrated that an increase in temperature leads to an increase in H_2 and CO concentration and to a decrease in CH_4 at equilibrium [4]. They examined the thermodynamic equilibrium of this system and suggested operating temperatures greater than 650K, atmospheric pressure and a molar ratio of ethanol/steam of 10 in the feed to maximize the production of H_2, minimize the formation of CO and CH_4 and avoid deposition of coke on the catalyst. Other authors [1] have also carried out a thermodynamic analysis of the system. They demonstrated that an increment in the total pressure led to decrease

*To whom correspondence should be addressed: Email: jlcl@correo.azc.uam.mx
Phone: 53189065 ext 116, Fax 53947378

NOMENCLATURE

Si (%)	Selectivity to product i
X	Conversion
Ni	Moles of product i
Nj	Moles of each product (included i)
K	Equilibrium constant
y_{CO2}	Mole fraction of CO_2
y_{H2}	Mole fraction of H_2
y_{H2O}	Mole fraction of H_2O
y_{OH}	Mole fraction of Ethanol
N_{OH}	Moles of ethanol during reaction
$N_{OH}°$	Initial moles of ethanol
N_{CO2}	Moles of CO_2 during reaction
N_{H2}	Moles of H_2 during reaction
N_{H2O}	Moles of H_2O during reaction
$N_{H2O}°$	Initial moles of H_2O
N	Total moles

of H_2 and CO while the composition of the CH_4 in the equilibrium increased. However the system of H_2 production and its purification has been operated at low pressure when the level of CO is reduced and the gas is rich in H_2 using a metallic membrane of Pd.

Some authors carried out a thermodynamic analysis of the ethanol-water system applied to a fuel cell and suggested that a high water-to-ethanol ratio in the feed reduced the yield of undesirable products such as CO, CH_4 and carbon [5].

The catalytic process has been studied by developing catalysts where different metals such as: Rh, Pt, Ni, Co, Zn, Fe, Cu, Au, Pd and Ru have been proven, with diverse supports of metallic oxides such as Al_2O_3 [6] CeO_2 [7], MgO [8], ZnO [9], SiO_2, Sm_2O_3, TiO_2, V_2O_5 [10] La_2O_3, Y_2O_3 [11], CeO_2-ZrO_2 [12] among other, some alkaline promoters as K, Na and Li have been proven [13].

From many investigations, we can deduce that the activity and the distribution of products depend on the type and concentration of used metal, of the support type and the preparation method. The biggest interest is to find active catalysts that inhibit coke formation and especially of the CO that is harmful for fuel cells [14]. Catalysts containing Co have showed a significant enhancement of the catalytic performance in the steam reforming of ethanol [10].

The hydrotalcites are materials of wide use in catalysis because they contain high specific area, they have the possibility of modifying their superficial characteristics and in consequence their catalytic properties, also these supports are not commonly used for the production of H_2 and they have basic sites, which are important to prevent the formation of CH_2=CH_2. The use of these hydrotalcites in ethanol steam reforming has been shown in other papers [15] and now in this study we combined tungsten oxides (WOx) with the Pt-hydrotalcite catalysts in order to thermal stabilize the porous structure [16,17].

Recently, some catalysts containing hydrotalcites or hydrotalcite-like compound precursors with new preparation methods have been reported to produce H_2. For example, Liu et al [18] prepared their solids using a combination of the reverse microemulsion (surfactant and hydrocarbon) and coprecipitation of the nitrates of Ni(II), Mg(II), Al(III) with $NaCO_3$ and NaOH solutions. It was observed that the precursor obtained from the above method possessed superior characteristics for preparing the mixed oxide catalyst used in ethanol steam reforming. The authors mentioned that the reverse microemulsion-derived catalyst showed much better catalytic performance than catalysts prepared from conventional coprecipitation or impregnation methods in terms of H_2 selectivity and catalyst stability.

Other authors [19] prepared catalysts with Ni loaded Mg-Al mixed oxide supported catalysts which were superior in H_2 and COx product selectivity and stability compared to the pure oxide supported Ni catalysts. Other authors using hydrotalcites with some compounds containing new elements (La,Ce,Zn,Co,Cu) produced a certain stabilization over the active metal phases with good selectivities to H_2 [20-23]. In this study the incorporation of WOx in the hydrotalcite obtained by coprecipitation is studied in order to stabilize the Pt particles over the catalysts.

2. EXPERIMENTAL

2.1. Catalysts Preparation

The hydrotalcite was made by co-precipitation using two salt solutions as precursors. First, in a stirred reactor one salt solution of Mg $(NO_3)_2$ and $Al_2(NO_2)_3$ (J.T. Baker) having an atomic ratio of Mg^{2+}/Al^{3+} of 2.1. A second solution of Na_2CO_3 (5%) and NaOH (pH = 10) (Carlo Erba) was prepared. These two solutions were mixed drop by drop in water (60 drops/min) at 60°C in a simultaneous manner in a third stirred reactor, the pH of the solution was measured. The catalysts were made adding $(NH_4)_{12}W_{12}O_{41}5H_2O$, (Aldrich) and H_2PtCl_6 in solution after the co-precipitation to get a constant amount of 0.35wt%Pt and several W concentrations: without W (sample HT), 0.5wt%W(sample HT05W), 0.5wt%W and Pt (HTP05W), 1wt%W and Pt (HTP1W), 2 and 3 wt% W and Pt (HTP2W and HTP3W). After this impregnation the solid suspension was stirred during 24 h at 60°C. The solid phase was washed three times with distilled water and it was dried at 120°C for 24 h and calcined at 450°C during 5 h. Finally the catalysts were reduced in H_2 at 450°C for 2 h.

2.2. Catalysts Characterization

The solids obtained were characterized by X-ray diffraction (XRD) in a Phillips X´ Pert instrument. The XRD patterns of the samples after calcination were obtained using the CuKα radiation. Diffraction intensity was measured in the 2θ range between 5 and 70° with a 2θ step of 0.02° with 8 seconds per point, the samples were analyzed directly at room temperature. The infrared spectroscopy was made in a Perkin Elmer spectrophotometer (Spectrum-RX). An infrared beam was sent through a wafer of the sample. The wavenumber range was from 4000 to 400 cm^{-1} and the number of averaged scans was 50. N_2 physisorption a - 196°C was made in a Micromeritics 2000 instrument. Each sample was pretreated at 200°C under vacuum (1 x 10^{-4} torr). The diffuse reflectance UV-visible spectroscopic analysis (UV-vis) of the samples was made in a Varian (Cary 5E) spectrophotometer. The range of wavelength

was from 3000 to 200 nm.

2.3. Catalytic evaluation

The catalytic evaluation of ethanol steam reforming was made in a U-shaped stainless steel fixed bed reactor (7 mm internal diameter). The catalyst (1g, 100 US mesh) was charged for each of the reaction tests. The feed of the reactants comprised of a gaseous mixture of ethanol (Aldrich), water as steam and N_2 (purity 99.99%, Infra-Air Products) was supplied by a micrometric needle valve (1 ml/s). A constant mixture H_2O and CH_3CH_2OH (molar ratio of 4:1) in a N_2 stream was supplied in gas flow using two glass saturators and this mixture was vaporized and kept at 92°C before it was feed to the reaction chamber.

The temperature of the catalyst was raised at 450°C in flow of N_2 for 30 min to activate the catalyst and then the flow of reactants started at this temperature. The catalyst was held at that temperature for 30 min in order to have three analyses and for deactivation tests the catalysts were evaluated during 300 min.

The analysis of the reactants and all the reaction products was carried out online by gas chromatography. Inside an automated injection valve, the sample was divided into two portions which were then analyzed in a different way in order to obtain accurate, complete quantification of the reaction products. One of the portions was used to analyze H_2, CO, CO_2 and CH_4, using a packed column of silica gel 12 grade 60/80 (18´x 1/8") with a thermal conductivity detector (Gow-Mac 550 apparatus). The second portion was used to analyze CH_3CH_2OH, CH_3CHO, CH_3COCH_3, CH_2O and $CH_2{=}CH_2$ with a capillary column (VF-1ms, 15m x 0.25 mm) in a Varian chromatograph CP-3380 with a flame ionization detector (FID). Response factors for all products were obtained and the system was calibrated with appropriate standards before each catalytic test. The conversion (X) was calculated using the ethanol composition before and after of the reaction. The selectivity was defined as the mole fraction of each product as follows:

$$Si\ (\%) = Ni / \Sigma\ Nj \times 100 \qquad (1)$$

The water was not included.

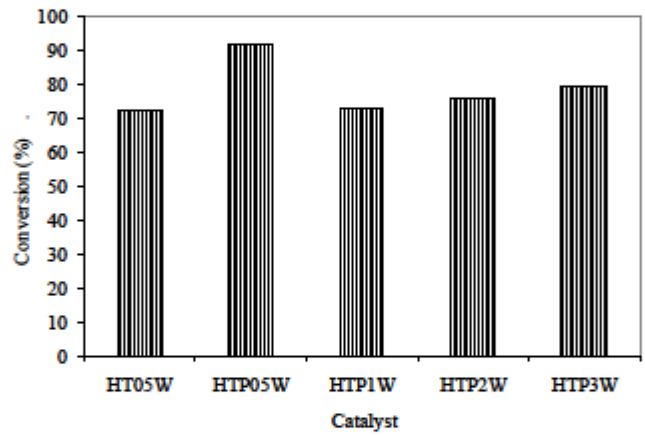

Figure 1 . Ethanol conversion for the Pt/WOx-hydrotalcite catalysts at 450°C after 7 h of reaction.

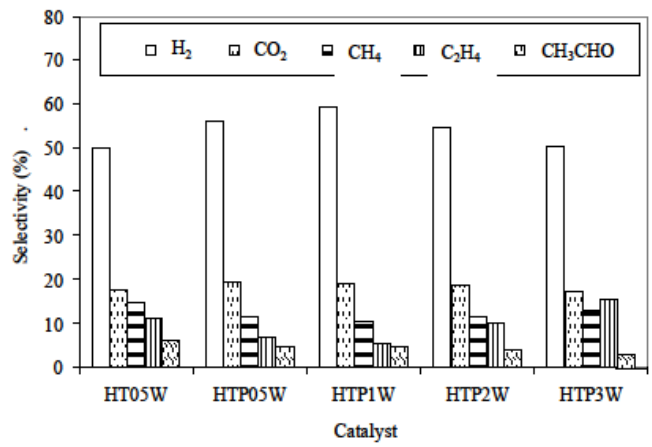

Figure 2. Selectivity of reaction products from ethanol steam reforming over Pt/WOx-Hydrotalcite catalysts at 450°C.

3. RESULTS AND DISCUSSION

3.1. Catalytic activity

These catalysts produced the following products of reaction: H_2, CH_3CHO, CO_2, CH_4, $CH_2{=}CH_2$ (Table 1). We did not find: CH_3COOH, $CH_3CH{=}CH_2$ or other oxygenates. For the all the samples, the presence of CO was very small or was not detected using the conductivity detector.

The sample HTP05W (0.5wt%W) showed an important promoting effect in conversion (Figure 1). For the other catalysts, the W addition to the hydrotalcite showed a small promoting effect.

The WOx/hydrotalcite without Pt (HT05W) showed catalytic activity of ethanol steam reforming (Figure 2). Also this type of hydrotalcite without W showed activity [15]. The formation of different species on the surface has revealed that the content of oxygen of different nature such as unidentate, bidentate and formation of bicarbonate species involved surface hydroxyl groups [24]. The presence of superficial –OH on the hydrotalcite catalyzed the initial interaction of ethanol with these –OH groups to form ethoxy

Table 1. Experimental mole fractions of the ethanol steam reforming over Pt-WOx-hydrotalcite catalysts.

Catalyst	CH_3CH_2OH	C_2H_4	CH_3CHO	H_2	CO_2	CH_4	H_2O
HT05W	0.118	0.148	0.130	0.337	0.046	0.069	0.149
HTP05W	0.109	0.096	0.117	0.375	0.068	0.083	0.148
HTP1W	0.089	0.041	0.103	0.397	0.106	0.090	0.160
HTP2W	0.085	0.087	0.098	0.379	0.096	0.084	0.159
HTP3W	0.074	0.116	0.091	0.371	0.095	0.072	0.176

species which could evolve to CH_3CHO, then this compound may either evolve over the surface through alkyl elimination or form a bidentate acetate species, which suffer a C-C scission on the surface of the hydrotalcite producing CO_2, CH_4 and H_2 in the presence of water [24]. This explanation could be similar for the steam reforming of ethanol using ZnO. This oxide showed catalytic activity producing H_2, CO_2 and CH_3CHO [24]. HT05W catalyst showed a selectivity of CH_3CHO near the 5% (Figure 2). In this point several reactions have been reported for ethanol steam reforming, they are as follows:

$$CH_3CH_2OH + 3\ H_2O \rightarrow 2\ CO_2 + 6\ H_2 \quad (2)$$

$$CH_3CH_2OH \rightarrow CH_3CHO + H_2 \quad (3)$$

$$CH_3CH_2OH + H_2O \rightarrow CO_2 + CH_4 + 2\ H_2 \quad (4)$$

$$CH_3CH_2OH \rightarrow CH_2{=}\ CH_2 + H_2O \quad (5)$$

$$CO + H_2O \rightarrow CO_2 + H_2 \text{ (water-gas shift reaction)} \quad (6)$$

$$CH_4 + H_2O \rightarrow CO + 3\ H_2 \quad (7)$$

$$CH_2 = CH_2 + 2\ H_2O \rightarrow CH_4 + CO_2 + 2\ H_2 \quad (8)$$

$$CH_3CHO \rightarrow CO + CH_4 \quad (9)$$

$$CH_3CHO + H_2O \rightarrow CH_4 + CO_2 + H_2 \quad (10)$$

$$CH_3CHO + H_2O \rightarrow 2CO + 3H_2 \quad (11)$$

Ethanol steam reforming (reaction 2) does not produce intermediate compounds and is considered the main reaction. In the case of CH_3CHO its selectivity decreased as W concentration increased (Figure 2) and we found this product in all the catalytic analyses. The presence CH_3CHO suggested that these catalysts acted as dehydrogenation catalysts following the reaction (3). In accordance with the reaction mechanism proposed by Frusteri et al. [8] (Figure 3) CH_3CHO is an intermediate product and the reactions (9), (10) and (11) could be feasible. The presence of CH_3CHO has been reported in ethanol steam reforming using several catalysts. For example in Ni-Mg-Al layered double hydrotalcites the selectivity was of 4% at 450°C [25], in Rh/MgO, Pd/MgO, Co/MgO and Ni/MgO reported among 5 and 19 %vol. [8]. The CH_3CHO selectivity was 4% and 3% on Ni/Y_2O_3, and on Ni/La_2O_3 respectively [11]. Also similar selectivities of CH_3CHO have been observed in our catalytic results (average of 5%). If we choose the reaction mechanism proposed by Frusteri et al. [8] (Figure 3), ethanol is firstly dehydrogenated to CH_3CHO which subsequently decomposes into CH_4 and CO (reaction 9). These last ones by steam reforming of CH_4 (reaction 7) and water gas shift reaction of CO (reaction 6) give rise to the formation of H_2 CO_2 and CO. Frequently, H_2, CO_2 and CH_4 are reported as final products which are favored through the excess of water in the system [26].

We did not find CO in the products distribution (Table 1). CO formation in not negligible during the steam reforming of ethanol and under our reaction conditions (450°C). The presence of 16 % of CO selectivity has been reported in the homogeneous (non-catalytic) reaction Laosiripojana [27]. Using several catalysts the presence of CO has been reported by Comas et al. [28], these authors obtained 14% using a Ni/Al_2O_3 catalyst. Another example

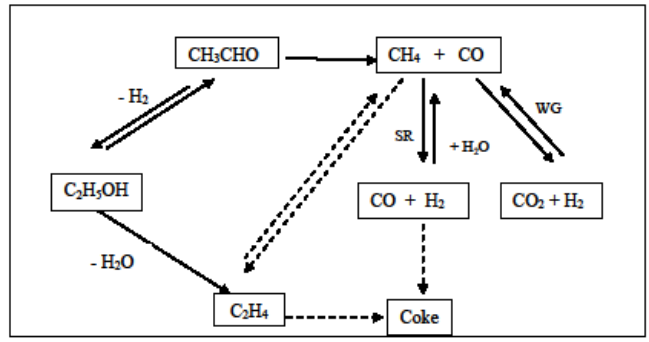

Figure 3. Reaction mechanism scheme of ethanol steam reforming proposed by Frusteri [8]. SR is steam reforming and WG is water-gas shift reaction.

was made by Homs et al. [9], using the Co-Cu-ZnO_2 catalyst (at 723K). They obtained a CO selectivity of 1%. Another example using noble metals (Ir, Ru, Pd, Pt) supported on Al_2O_3 and CeO_2 was made by Erdohelyi et al. [29]. They reported CO selectivities between 5 and 11%.

The catalyst HT05W (free of Pt) showed the highest selectivity to $CH_2{=}CH_2$ (Figure 2). The ethanol dehydration to the olefin, (reaction 5) was affected by the presence of Pt. In accordance with Frusteri et al.[8], ethylene and acetaldehyde are intermediate products formed from ethanol dehydration and dehydrogenation respectively, reaction (5) and reaction (3) (Figure 3). These products can promote coke formation [30].

Yields of these products as a function of space time or the gas hour space velocity (GHSV) have a typical behavior of intermediate products [28]. For example, Llorca et al. [10] found that the acetaldehyde selectivity decreased from 1.6 to 0.5% as the GHSV increased. At space times lower than 0.5 (ml of total flow in the inlet/(mg of catal.)(min)) ethylene and acetaldehyde appeared within the reaction products in low selectivity.

The difference in H_2 selectivity between the HTP1W catalyst and the others was very small. It is known, that the H_2 production comes from several reactions; dehydrogenation, water-gas shift conversion of CO and decomposition of oxygenated compounds. In this way, infrared studies have showed that dehydrogenation of molecularly adsorbed ethanol was proposed as a key reaction step [29]. The ethanol adsorbs molecularly to form hydrogen-bonded weakly adsorbed species and to produce strongly adsorbed molecular ethanol on the Lewis-sites of the support. It was found that at high temperature treatment of the adsorbed species produce the formation of surface acetate species on the support and the decomposition of the ethoxide species (at the metal/support interface) led to the formation of H_2 [29].

Also it was found that presence of water lowered the temperature at which the acetate species appeared and increased the stability of monodentate ethoxide species and the dehydrogenation of ethanol proceeded on the Pt metal producing H_2 and carbonyl-hydride surface species.

3.2. Equilibrium calculations

To get an idea of the approach to equilibrium, we performed

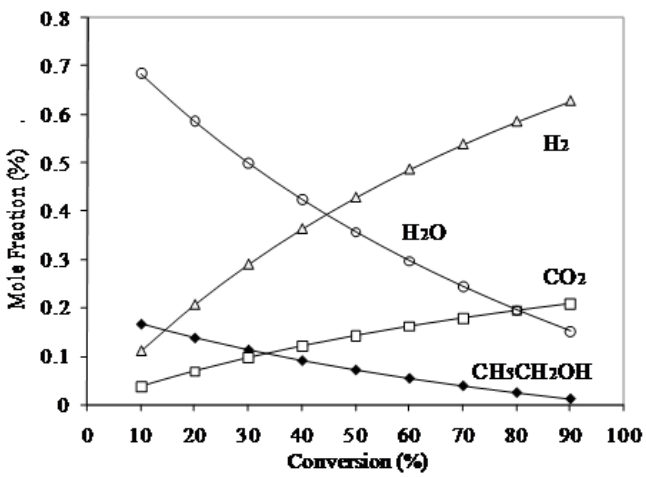

Figure 4. Mole fractions yi for each reaction product in the equilibrium calculated from de Equation (12).

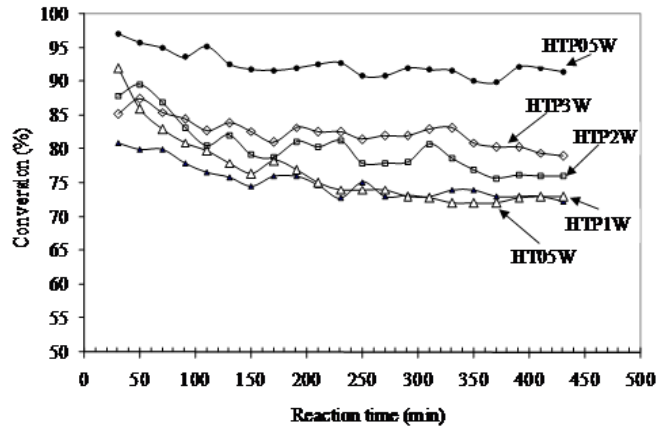

Figure 5. Catalytic deactivation of the Pt/WOx-Hydrotalcite catalyst at 450°C in the ethanol steam reforming.

calculations considering the reaction (1) which represents the main contribution in the system [31]. Figure 4, shows the equilibrium mole fractions for the different components calculated from equation 1 using equations 10-18 to define mole fractions. We considered the 4:1 molar flow ratio of water to ethanol.

$$K = \frac{y_{CO_2}^2 y_{H_2}^6}{y_{H_2O}^3 y_{OH}} \quad (12)$$

The mole balance of the reaction (1) where X is conversion was as follows:

$$N_{OH} = (N_{OH}° - N_{OH}° X) \quad (13)$$

$$N_{CO2} = N_{OH}° 2X \quad (14)$$

$$N_{H2} = N_{OH}° 6 X \quad (15)$$

$$N_{H2O} = (N_{H2O}° - N_{OH}° 3X) \quad (16)$$

$$N = \text{Total moles} = N_{OH}° + 4N°_{OH}X + N_{H2O}° \quad (17)$$

The mole fractions were:

$$y_{OH} = (N_{OH}° - N_{OH}° X) / N \quad (18)$$

$$y_{CO2} = (N_{OH}° 2X) / N \quad (19)$$

$$y_{H2} = (N_{OH}° 6 X) / N \quad (20)$$

$$y_{H2O} = (N_{H2O}° - N_{OH}° 3X)/ N \quad (21)$$

The experimental and equilibrium mole fractions for H_2, CO_2, and H_2O were compared (Table 2). The calculated mole fractions for the products H_2 and CO_2 were higher than the experimental fractions. This is because the other experimental product mole fractions (CH_3CHO, $CH_2{=}CH_2$ and CH_4) were not added. In the case of water, the differences between experimental and calculated mol fractions were small, because this reactant was in excess with respect to ethanol. Calculations of the equilibrium mole fractions of all the reaction products will be made in the future.

3.3. Catalytic Stability

The catalyst HTP05W (with 0.5wt%W and Pt) showed the largest stability after 7 h at 450°C (Figure 5). This behavior was very similar with the W effect in catalysts supported on Al_2O_3 [16, 17]. It was observed that catalysts with a concentration of W below of monolayer, were stabilized and probably the Pt sinterization process was reduced. A thermal stabilization effect of W over Pt particles could be the explanation [16,17]. In this study the addition of W to the hydrotalcite promoted (at low W concentration) both the conversion and stability.

Table 2. Experimental and equilibrium mole fractions of some reaction products (considering only products of reaction (1)) over Pt/WOx-hydrotalcite catalysts at 78% conversion.

Catalyst	C_2H_5OH		H_2		CO_2		H_2O	
	Exper.	Calculated	Exper.	Calculated	Exper.	Calculated	Exper.	Calculated
HT05W	0.118	0.04	0.337	0.58	0.046	0.20	0.149	0.20
HTP05W	0.109	0.04	0.375	0.58	0.068	0.20	0.148	0.20
HTP1W	0.089	0.04	0.397	0.58	0.106	0.20	0.160	0.20
HTP2W	0.085	0.04	0.379	0.58	0.096	0.20	0.159	0.20
HTP3W	0.074	0.04	0.371	0.58	0.095	0.20	0.176	0.20

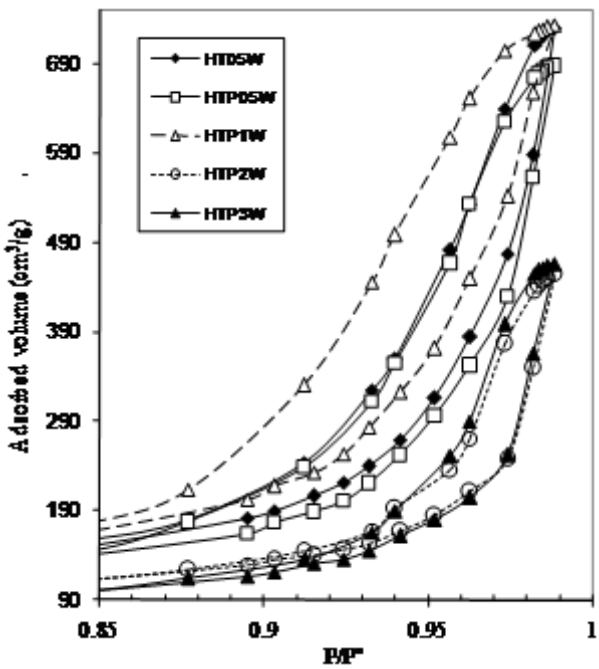

Figure 6. N_2 isotherms of the Pt /WOx-Hydrotalcite catalysts.

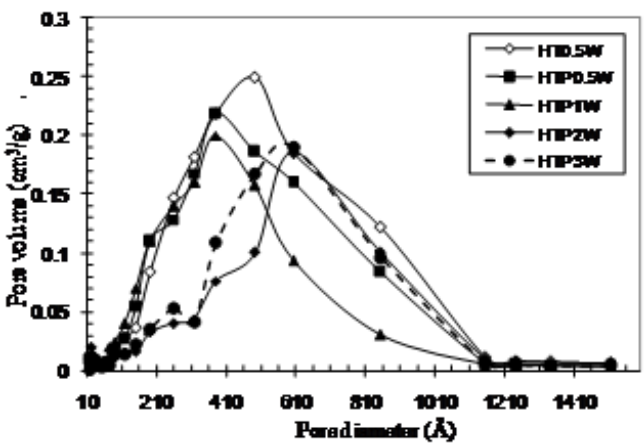

Figure 7. Pore distribution of the Pt /WOx-Hydrotalcite catalysts.

Table 3. Surface area and pore diameter of the Pt/WOx-Hydrotalcite catalysts. The Pt concentration remained constant in 0.35wt%.

Catalyst	W (% peso)	Surface Area BET (m^2/g)	Pore Volume (cm^3/g)	Pore Diameter (Å)
HT05W	0.5	257	1.1	175
HTP05W	0.5	227	1.0	186
HTP1W	1	242	1.1	187
HTP2W	2	229	0.7	122
HTP3W	3	151	0.7	191

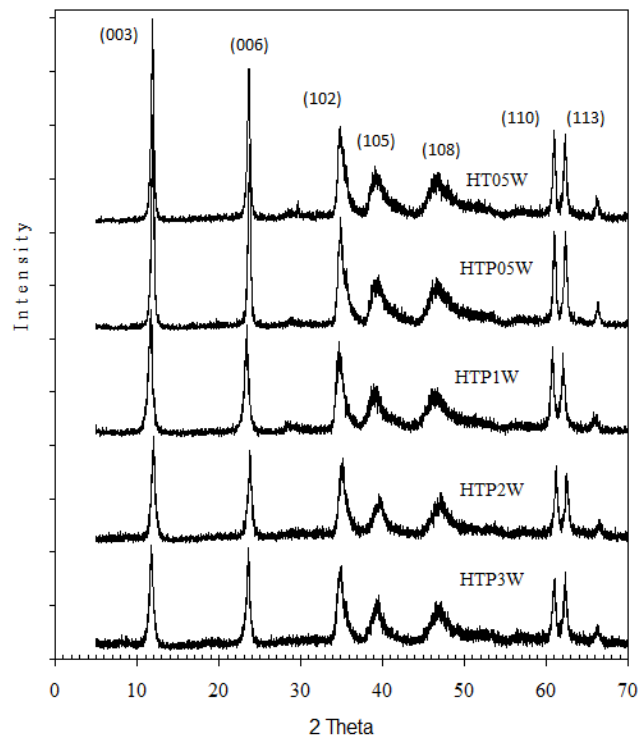

Figure 8. X-ray diffraction of the Pt/WOx-Hydrotalcite catalysts.

3.4. Textural properties

Both, the surface area BET and the nominal content of W are shown in Table 3. N_2 Isotherms at -196°C for samples HT05W to HTP3W are shown in Figure 6. They show the type IV pattern of the IUPAC classification [32] with a rather small hysteresis loop (type H3). According with IUPAC this type of loop corresponds with a porous material composed by slit-shaped pores with parallel walls. The loops close at a relative pressure of 0.85 for most of the samples, indicating similar pore architecture of mesoporous dimensions. These results are further corroborated by the pore size distribution of the samples (Figure 7). In general, pore formation in hydrotalcites is through interparticle packing and the distribution of pores is influenced by the crystallite size and packing arrangement of crystallites [25]. A relative narrow distribution of mesopores was observed for HTP2W and HTP3W samples whereas a broader distribution of mesopores prevails for HT0.5W, HTP0.5W and HTP1W samples. This interparticle packing is reflected in the calculus of average pore diameter (computed from the desorption branch of the isotherm) for the samples HT05W (175 Å) and HTP3W (191 Å) (Table 3) and with the specific surface area of the former which is 1.7 times higher than the latter. The total pore volume, specific surface area and the area of the hysteresis loop decreases when the W content increased. These results are similar to those reported previously for Co/WOx-Hydrotalcite [33] and Pt-W-Hydrotalcite and Pt-Mo-Hydortalcite [34] and Pt-hydrotalcite [35]. These changes in texture probably originated from morphological differences in the hydrotalcite crystallites arising with the change in WOx concentration.

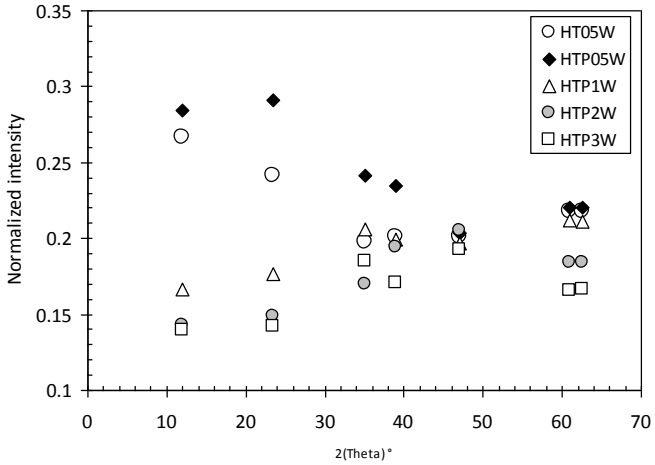

Figure 9. Normalized Intensity of reflections produced by Pt/WOx-Hydrotalcite catalysts from XRD.

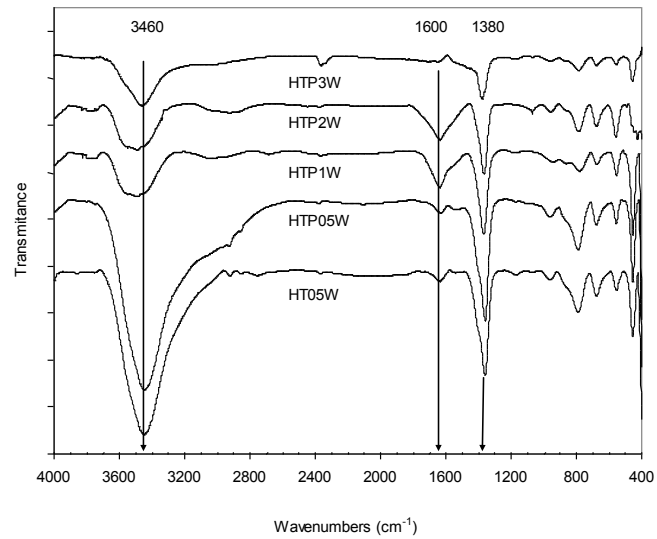

Figure 10. Infrared spectra of Pt/WOx-hydrotalcite catalysts.

3.5. XRD analysis

The Figure 8 shows the XRD patterns of the samples having Pt with a constant 0.35wt% (HTP05W to HTP3W) and the sample free of Pt with 0.5%W (HT05W). The diffraction patterns recorded of all the samples are typical of the hydrotalcite-like structure with hexagonal unit cell [15, 36]. They were identified from the JCPDS file and the 022-0700 card. All samples crystallized in only the hydrotalcite phase, indicating that the incorporated metals (W or Pt) into the hydrotalcite support did not destroy its structure. The peaks were indexed with the proper Miller indices. It was found symmetric intense peaks in reflections 2θ located in (003), (006), (110) and (113) and asymmetric peaks in (012), (015) and (018). The Figure 8 revealed that as W concentration increased the crystalline structure of the hydrotalcite samples changed. The peak intensity decreased and it was a broadening of the peaks, which were associated to a decreasing of the crystalline perfection and to the introduction of lattice defects, attributed to the non-stoichiometric nature and partially disordered structure. The absence of other phases suggests that both W^{6+} and Al^{3+} have isomorphically replaced Mg^{2+} cations in the burcite-like layers [33]. In order to quantify these changes, the intensity of all diffraction lines were normalized as W concentration increased (Figure 9). The (003) and (006) reflections showed the highest changes. The normalized intensity of reflections (003) and (006) for samples HTP1W, HTP2W and HTP3W decreased respect to those of samples HTP05W and HT05W. In other words very low W concentrations of W (0.5%W) almost did not change the crystallinity of the hydrotalcite. Moreover the (003) and (006) normalized intensities of HTP05W catalyst were superior to those of HT05W catalyst. From Figure 9 this observation was more evident with the (006) reflection. In fact, this HTP05W catalyst (having Pt) showed the highest normalized intensity respect to all the samples and therefore it was the more crystalline. In general the addition of W ions to the hydrotalcite in amounts less than 3% did not change their crystal reflections respect to hydrotalcite X-ray pattern [28]. The lost of crystallinity due to the addition of W ions (reflected in the normalized intensity) to the hydrotalcite phase was similar with the presence of Ni [32] or Co [15]. These substitutions lead to the introduction of micro strain on the crystalline lattice. We found that catalyst with high crystallinity (the sample HTP05W) showed the highest stability after 420 min at 450°C. It could be a possible thermal stabilization effect of W in the hydrotalcite lattice leading to prevent the Pt sintering [16,17].

3.6. Infrared analysis

The infrared spectra of the samples showed a broad stretching band in the region 3400-3000 cm^{-1} attributed to –OH functional groups and a H_2O scissoring mode band near 1600 cm^{-1} which provide evidence of the presence of water molecules (Figure 10). In the –OH stretching region we expect three features in IR spectra, i.e. the antisymmetric –OH stretching of the brucite-type layers and the antisymmetric and symmetric stretching of water molecules. Some authors have attributed the band at 3410 cm^{-1} with hydroxil groups coordinated with Mg and Al while the vibration of the same group associated with water is a wide band between 3650-3590 cm^{-1} [37]. The antisymmetric -OH stretching band located at 3460 cm^{-1} of the brucite type layers decreased as W concentration was from 0.5wt% (sample HTP05W) to 1 and 2 wt% (samples HTP1W and HTP2W). The analysis of the W effect on the superficial species suggested that W decreased the –OH groups of the brucite type layers. The sample HTP05W (having Pt and the lowest amount of W) showed the highest signal for the hydroxil groups. The next strong band was located at 1380 cm^{-1} which is attributed to the co-presence of carbonate ions (broad antisymmetric stretching at 1360 cm^{-1}) and residual nitrate ions (sharp antisymmetric stretching at 1380 cm^{-1})[[25]. Another band located at 1029 cm^{-1} is related with the symmetric C=O stretching carbonate ion which has been found in the band 1041cm^{-1} [25]. In the region below 1000 cm^{-1} the spectrum showed a band located in 772 cm^{-1} which is related with vibrations of –OH bending of brucite type layers [25]. Finally, the bands located at 680, 560 cm^{-1} are related with vibration modes of brucite type layers specifically the metal-oxygen symmetrical stretching.

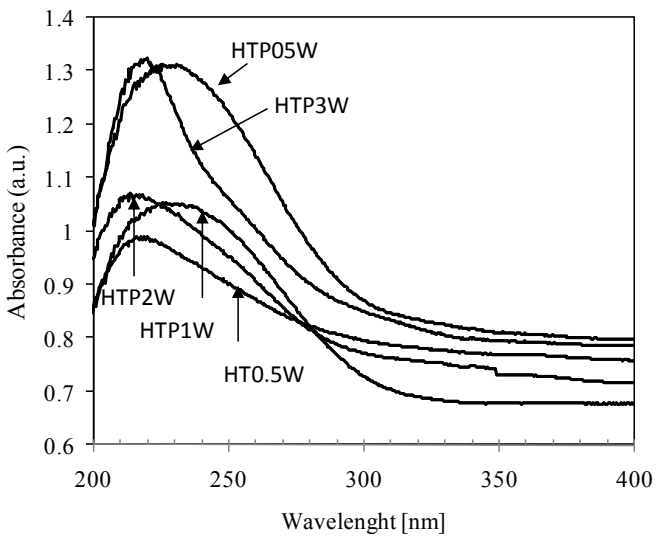

Figure 11. UV-vis spectra of the Pt/WOx-Hydrotalcite calcined.

3.7. UV-vis analysis

The sample HT0.5W (without Pt) showed a band with a maximum at 215 nm (Figure 11). This band has been attributed to a ligand-metal charge transfer (LMCT) of the single ligand of the W=O (the W^{6+} is a cation d°) [38,39]. Usually this band increased as the W concentration increased on Al_2O_3. This behavior was observed in samples HT05W, HTP2W and HTP3W suggesting that W^{6+} ions are present in a tetrahedral coordination [40-42]. It is known that the structure of tungstated ion in aqueous solution is highly dependent of the pH and in alkaline solutions the W^{6+} ion could be present as a tetrahedral monomeric ion $[WO_4]^{2-}$ [43].

From Figure 6, the sample HTP05W (with Pt) showed a strong and wide band located between 210 to 300 nm related with the combination of Pt and W signals. This sample showed the main absorbance located at 230 nm. In order to explain this band, Jackson et al [44] and Lever et al., [45] have found bands located at 217 nm and 210 nm respectively. These bands have been attributed to a ligand-metal charge transfer of the ligand [O] to octahedral Pt^{4+} cation which is due to the presence of a compound of type $[PtCl_5OH]^{2-}$. Other authors [46] have reported a similar band at 270 nm when the calcination temperature was 300°C using H_2PtCl_6 as precursor of Pt species on Al_2O_3. Samples containing low W concentrations with Pt (HTP0.5W and HT1W) showed wide bands which could include the another bands due to Pt^{4+} ions reported by Lietz et al.[46]. Therefore the spectrum of the sample HTP0.5W corresponded with the catalyst showing the most important signal due to a LMCT and d-d signals of Pt^{4+} ions. In other words, this sample showed the most important amount of Pt on the surface of the hydrotalcite.

From the UV-vis spectra we can observe that HTP05W catalyst showed the most important signals of Pt and W. Therefore this catalyst could have the most important amount of Pt on the surface of the hydrotalcite and as a consequence the most stability to deactivation because the presence of Pt crystallites catalyzed the coke precursors.

4. CONCLUSIONS

It was found a promoter effect of W on the Pt/WOx-hydrotalcite catalysts. The addition of W in low amounts (0.5 and 1wt%W) produced high thermal stability and high H_2 selectivity. As W concentration increased, both the intensity of crystalline reflections of the catalysts and the conversion increased. The catalysts did not produce CO and showed low selectivity to CH_2=CH_2. These enhanced catalytic properties were related with a better WOx-Hydrotalcite crystallinity and the possible Pt stabilization produced by the W^{6+} ions bonded with the hydrotalcite structure. It was found superficial chemical groups as: H_2O, Al-OH, Mg-OH, and CO_3^{2-}. The Pt/WOx-hydrotalcite catalyst with the lowest W concentration (0.5wt%) showed the highest catalytic stability because only at this concentration of W there were enough Pt species on the hydrotalcite surface.

We found that catalysts with low W concentration and Pt having high crystallinity (sample HTP05W) showed the highest stability after ethanol steam reforming. It could be a possible thermal stabilization effect of W in the hydrotalcite crystal structure leading to prevent the Pt sintering.

5. ACKNOWLEDGEMENTS

The authors acknowledge the financial support of the Universidad Autónoma Metropolitana-Azcapotzalco, Iztapalapa, the Instituto Politécnico Nacional and the Instituto Mexicano del Petróleo.

REFERENCES

[1] F. Aupretre, C.Descorme, D.Duprez, D.Casanave.D. Uzio, J. Catal., 233, 464 (2005).

[2] E.Y. García, M.A. Laborde, Int. J. Hydrogen Energy, 16, 307 (1991).

[3] K. Vasudeva, N. Mitra P., S. Umasankar, C. Dhingra, Int. J. Hydr. Energy, 21, 13 (1996).

[4] I. Fishtik, R. Alexander, R. Datta, R.D. Geana, Int. J. Hydrogen Energy, 25, 31 (2000).

[5] S. Freni, G. Maggio, S. Cavallaro, J. Power Sources, 62, 67 (1996).

[6] J.P. Breen, R. Burch, H.M. Coleman, Appl. Catal. B:Environ, 39, 65 (2002).

[7] N. Laosiripojana, S. Assabumrungrat. Appl. Catal. B:Environ, 669, 29 (2006).

[8] F. Frusteri, S. Freni, V. Spadaro, Chiodo, G. Boura, S. Donato, S. Carvallo, Catal. Commun., 5, 611 (2004).

[9] N. Homs, J. Llorca, P.Ramírez de la Piscina, Catal. Today, 116, 361 (2006).

[10]J. Llorca, N. Homs, J. Salts, P.Ramírez de la Piscina, J. of Catal., 209, 306 (2002).

[11]J. Sun, P. Xin, W.Q. Feng, Int. J. Hydrogen Energy, 30, 437 (2005).

[12]C. Diagne, H. Idriss, A. Kiennemann, Catal. Communications, 3, 565 (2002).

[13]C.L. Hernández and V. Kafarov. Proceedings of Simposio Iberoamericano de Catálisis Anais do XXSICAT, FISOCAT, Gramado Brazil, Sept 17-22. p1-8, 2006.

[14]V. Mas, M.L. Dieuzeide, R. Tejeda, M. Jobbagy, G. Baronetti, N. Amadeo, M. Laborde, Proceedings of Simposio Iberoamericano de Catálisis. Anais do XX SICAT –FISOCAT, Gramado, Brazil, Sept. 17-22, 2006.

[15]J.L. Contreras, J. Salmones, L.A. García, A. Ponce, B. Zeifert and G.A. Fuentes, J. of New Materials for Electrochemical Systems, 11, 109 (2008).

[16]J.L. Contreras, G.A. Fuentes, J. Salmones, B. Zeifert, J. of Alloys and Compounds, 483, 371 (2009).

[17]J.L. Contreras, G.A. Fuentes, J. Salmones, B. Zeifert. Mater. Res. Soc. Symp. Proc. Vol. 1279, Materials Research Society, 123 (2010).

[18] L. Liu, D. Chen, K. Zhang, J. Li, N. Shao, Int. J. of Hydrogen Energy, 33, 3736 (2008).

[19]L.J.I. Coleman, W. Epling, R.R. Hudgins, E. Croiset, Appl. Catal., A:General, 363, 52 (2009).

[20]L. He, H. Berntsen, De Chen, J. of Phys. Chem., A, 114, 3834 (2010).

[21]A.F. Lucrédio, J.D.A. Bellido, E.M. Assaf, Appl. Catal., A:General, 388, 77 (2010).

[22]G. Zeng, Q. Liu, R. Gu, L. Zhang, Y. Li, Catal. Today, (2011).

[23]R. Guil-López, R.M. Navarro, M.A. Peña, J.L.G. Fierro, Int. J. of Hydrogen Energy, 36, 1512 (2011).

[24]J. Llorca, N. Homs, P. Ramírez de la Piscina, J. of Catal., 227, 556 (2004).

[25]C. Resini, T. Montanari, L. Barattini, G. Ramis, G. Busca, S. Presto, P. Riani, R. Marazza, M. Sisani, F. Marmottini, U. Costantino, Appl. Catal. A:General, 355, 83 (2009).

[26]H. Vieira F., L.F. Dias P., Appl. Catal. A:General, 306, 134 (2006).

[27]N. Laosiripojana and S. Assabumrungrat, Appl. Catal. B:Environmental, 66, 29 (2006).

[28]J. Comas, F. Mariño, M. Laborde, N. Amadeo. Chem. Eng. J. 98, 61 (2004).

[29]A. Erdohelyi, J. Rasko, T. Kecskes, M. Toth, M. DömÖk, K. Baán, Catal. Today, 116, 367 (2006).

[30]J.R. Rostrup-Nielsen, N. Hojlund in: J. Oudar, H. Wise (Eds.), Deactivation and Poisoning of Catalyst, Marcel Dekker, New York, Basel, p.57, 1985.

[31]J.L. Contreras, M.A. Ortiz, G.A. Fuentes, R. Luna, J. Salmones, B. Zeifert, L. Nuño and A.Vázquez, J. of New Materials for Electrochemical Systems, 13, 253 (2010).

[32]T. Shishido, M. Sukenobu, H. Morioka, R. Furukawa, H. Shirahase, K. Takehira, Catal. Lett., 73, 21 (2001).

[33]A.C.C. Rodríguez, C.A. Enríquez, J.L.F. Monteiro, Mater. Res., 6, 563 (2003).

[34]S. Hamada, S. Hibarino, K. Ikeue, M. Machida, Appl. Catal. B: Environmental, 74, 197 (2007).

[35]F. Basile, G. Fornasari, M. Gazzano, A. Vaccari, Appl. Clay. Sci., 16, 185 (2000).

[36]I.O. Cruz, N.F.P. Ribeiro, D.A.G. Aranda, M.M.V.M. Souza, Catalysis Comm., 92606, 2611 (2008).

[37]María de los Ángeles Ocaña Zarceño, Síntesis de Hidrotalcitas y Materiales Derivados: Aplicaciones en Catálisis Básica. Tesis de Doctorado, Universidad Complutense de Madrid (2005).

[38]A. Bartecki and Dembicka, D.J. of Inorg. and Nuclear Chem. 29, 2907 (1967).

[39]J.L. Contreras and G.A. Fuentes, Studies in Surface Science and Catalysis, Vol.101 Edit. B. Delmon and J.T. Yates, Elsevier, 1195 (1996).

[40]A. Iannibello, L. Villa and S. Marengo, Gazzetta Chimica Italiana, 109, 521 (1979).

[41]L. Salvati, L.E. Makovsky, J.M. Stencel, F.R. Brown, D.M. Hercules, J. Phys. Chem., 85, 3700 (1981).

[42]J.A. Horsley, I.E. Wach, J.M. Brown, G.H. Via, F.D. Hardcastle, J. Phys. Chem., 91, 4014 (1987).

[43]W.P. Griffith and T.D. Wickins, J. Chem. Soc., A., 1087 (1966).

[44]Jackson, S.D. Glanville, B.M. Willis, J. McLellan, G.D. Webb, G, Moyes, R.B., Journal of Catal., 207 (1993).

[45]Lever A.B.P., "Inorganic Electronic Spectroscopy",2nd. Ed., Sud. Phys. Theor. Chem.33, Elsevier, Amsterdam, 1984.

[46]Lietz G., Lieske H., Spindler H., Hanke W. and Volter J., J. of Catal., 81, 17 (1983).